Application of seismic inversion and neural network for mapping reservoir properties in Raniganj coalfield, India

Dr. Abir Banerjee
Email: banerjee_abir@ongc.co.in, Oil and Natural Gas Corporation Limited

Abstract

Reservoir characterization for the lithological formation assesment is attempted in the Raniganj coalfield located in eastern part of India. Based on availability of 3 well logs and a two-dimensional post-stack seismic data, model-based post-stack seismic inversion is carried out to generate acoustic impedance section. Moreover, the seismic attributes obtained from the inversion are implemented in neural network architectures to map shale volume, Young's modulus, and Poisson's ratio. Error analysis between predicted and actual results demonstrates multi-layered feed-forward or probabilistic neural networks display a better result in obtaining reservoir parameters. The mapped reservoir section shows the acoustic impedance varying from 5000 to 16,000 (g/cc)*(m/s), shale volume ranging from 15% to 55%, Young's modulus, and Poisson's ratio varying from 0.5-9.5 GPa and 0.23-0.27 respectively. Cross-plot between Young's modulus versus Poisson's ratio classifies lithology from brittleness and it increases with depth. Neural network architectures help to identify the best model for delineating shale barriers for designing hydraulic fracturing treatments. Results from this study have added significant value to engineering applications and will help in ongoing coalbed methane exploration and future geomechanical studies. However, presence of cultural noise in seismic data adds limitations in resolving thin coal seams as the seismic resolution depends on the wavelength, velocity, and frequency of waves in the formation.

Introduction

The petrophysical parameters derived from the wireline log and seismic data provide sub-surface rock and fluid information. The log data are acquired in the depth domain whereas seismic data are recorded in the time domain. Both domains have some advantages and limitations. Well log data have higher resolution and provide less areal coverage whereas seismic data provides a much lower resolution with a greater areal extent. Therefore, combining well log and seismic data gives a finer description of reservoir properties on a wider scale (Hampson et al., 2001). The seismic section provides structural information about the fault and bedding plane but, the prime input for quantitative interpretation of subsurface formation is obtained from well log analysis and seismic inversion. Numerous seismic inversion methods are used such as maximum likelihood inversion, approximation computation, spars spike, band-limited impedance, Bayesian regularization, and model-based inversion. Among these methods, model-based inversion is widely used because it estimates the absolute acoustic impedance with greater correlation and maps the low-frequency content beyond the seismic band by using a bandpass filter (Mallick, 1995). Seismic inversion generates attributes by applying the mathematical transform that contains meaningful information and provides a better understanding of the reservoir properties. The geostatistical approach uses a linear relationship for integrating seismic attributes and reservoir parameters but it does not consider a non-linear relationship, whereas the application of neural network (NN) proves effective in dealing with the complex problem by using a non-linear relationship (Saggaf et al., 2003). Amongst numerous NN architectures developed, we are discussing multi-layered feed-forward neural network (MLFN) and probabilistic neural network (PNN) in this paper. However, the selection of the best model from several mathematical models with the same output remains the most crucial task for geoscientists. In the Raniganj basin, very limited studies are found in the literature related to mapping reservoir properties using seismic inversion and NN architectures with associated challenges. Hence, the main aim of the study includes (i) reservoir characterization from model-based seismic inversion, (ii) mapping of reservoir properties using NN architectures, and (iii) geological and engineering analysis for implications of hydraulic fracturing treatments in reservoir development and, (iv) associated challenges and limitations in resolving of thin coal seams.

Geological Setting and Datasets of the study area

Raniganj basin is part of peninsular India is mainly located in the state of West Bengal. The basin has an extension of 3000 km^2 containing sediments of lower and upper Gondwana. Structurally the basin is elongated semi-elliptical in shape along the E-W direction and shows a typical half-graben configuration. The boundary and intrabasinal faults are the major faults in the basin (Ghosh, 2002). The Salma dyke observed and move towards NNW-SSE to NW-SE direction is a significant igneous intrusion that divides the basin into two equal parts (Figure 1). The formations from the bottom of the reservoir include Basement, Talchir, Barakar, Barren measure, Raniganj, Panchet, and Supra-Panchet (Banerjee and Chatterjee, 2021). The Raniganj basin hosts commercial coal deposits in both Barakar and Raniganj formations. The study area contains wells named W1, W2 and W3, and only one 2D post-stack time migration seismic section (S3) along the NW-SE direction is available. In both wells (W1 and W2), geophysical logs- gamma-ray (GR), resistivity (RES), P-wave slowness (DTC), and density (DEN) are recorded, while neutron (NEU) is has been recorded well W2. In another nearby well W3, both P-wave slowness (DTC) and S-wave slowness (DTS) are available. The coal seams are distinguished from other lithology based on cut-off criteria from geophysical well logs, and acoustic impedance (AI), Young's modulus (E), and Poisson's ratio (PR) derived from well log.tabulated in Table 1.

Table 1. The distinction of lithology based on cut-off criteria based on well logs parameters and acoustic impedance (AI), Young's modulus (E), and Poisson's ratio (PR) derived from well log.

Lithology	GR (API)	RES (Ohm-m)	DEN (g/cc)	NEU (v/v)	P-wave (m/s)	AI (g/cc*m/s)	E (GPa)	PR
Coal	20-40	500-5000	1.4-1.8	0.50-0.70	2775-4285	5000-6000	0.5-2.5	0.26-0.30
Sandstone	55-65	45-70	2.5-2.6	0.08-0.1	2115-4000	5500-10000	2.5-6.0	0.22-0.26
Shale	115-160	25-30	2.55-2.6	0.32-0.33	3840-6270	10000-16000	7.0-12.0	0.16-0.22
Igneous intrusive	100-200	5-15	2.6-2.8	0.13-0.22	3240-3500	8420-9800	1.5-3.5	0.20-0.31

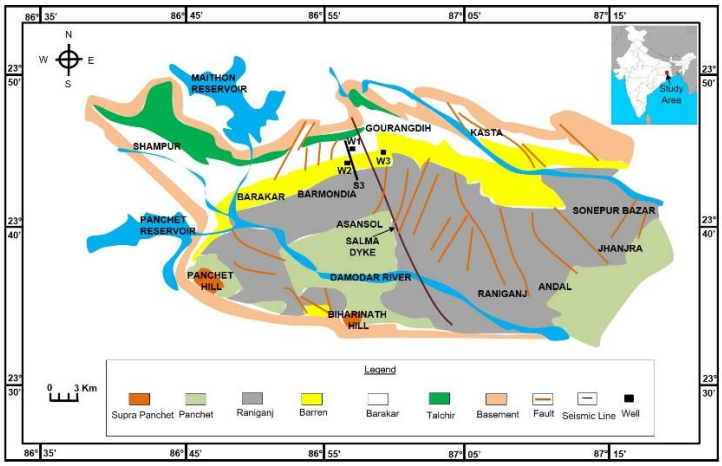

Figure 1. Geological map of the study area representing the geological formation, seismic line, and wells.

Methods

The 2D seismic data acquired in the Raniganj basin is intensively covered with coal mines activities, thickly populated townships, villages, and other logistics. The data was acquired in symmetrical split spread geometry with shot interval 10m, receiver interval 5m with 300 receivers on both sides of the shot was designed for higher foldage of 150 and closer spatial sampling. The data was recorded for 6 seconds in a high-frequency spectrum of a 1 ms sampling interval. The recorded data quality in the entire area is

significantly affected by the presence of cultural noise that has been generated from man-made activities such as automobiles, electric lines, industrial activities, steel pipelines, trains, and highways. The methodology presented in figure 2 illustrates the estimation of reservoir parameters such as shale volume, Young's modulus, and Poisson's ratio from well log and seismic data by implementing model-based post-stack seismic inversion and NN architecture. Also, the detailed steps followed in model-based post-stack seismic inversion are shown in the flowchart. The steps in the flowchart are described in the sub-sections.

Parameters estimation

The shale volume (V_{sh}) is determined from the GR log based on equation (Bateman, 1985):

$$V_{sh} = (GR_{\log} - GR_{\min}) / (GR_{\max} - GR_{\min}), \quad (1)$$

where GR_{log}, $GR_{min,}$ and GR_{max} are gamma-ray log magnitude in the formation (API units), clean sand, and shale. Young's modulus is defined from the ratio of linear stress by strain and the ratio of transverse to axial strain determines Poisson's ratio. In an isotropic homogeneous medium, dynamic Young's modulus (E) and Poisson's ratio (PR) in rocks are mathematically expressed as (Boonen, 2003):

$$E = \frac{\rho V_s^2 (3V_p^2 - 4V_s^2)}{V_p^2 - V_s^2}, \quad (2)$$

$$PR = \frac{(V_P / V_S)^2 - 2}{2*(V_P / V_S)^2 - 2}, \quad (3)$$

where ρ represents the density of the formation. The limitations of V_s log are a constraint in obtaining dynamic relationships. Therefore, based on available data in a nearby well W3, a linear relationship between Vp (Km/s) and Vs (Km/s) is obtained with 0.84 as a fitting coefficient (R^2) (Figure 3). The relationship between Vp and Vs is as follows:

Vs = 0.587 * Vp – 0.0869, (4)

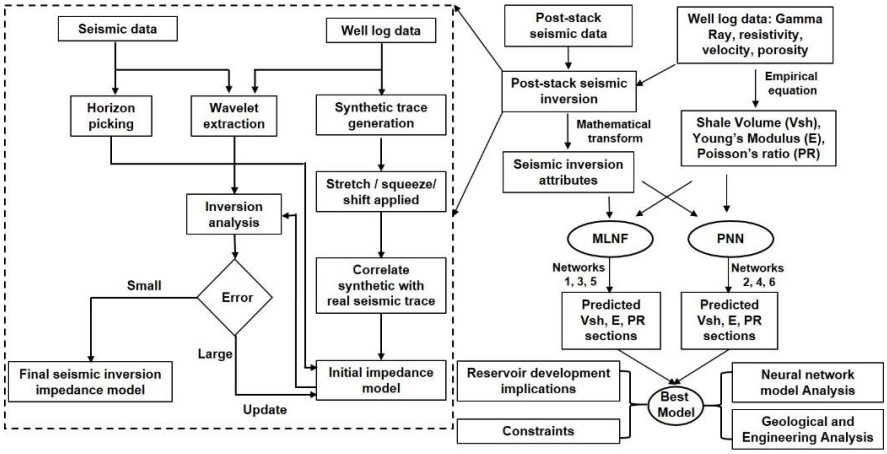

Figure 2. Flowchart of the study.

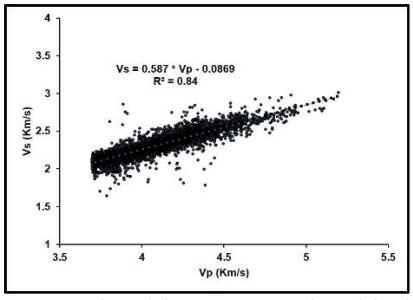

Figure 3. Cross-plot between Vp (Km/s) versus Vs (Km/s) showing linear relationship.

Model-based seismic inversion

Seismic inversion is a mathematical operation of converting reflected acoustic signal in the form of seismic trace, amplitude, and phase into the rock properties such as acoustic impedance (AI), velocity, and density. The transformation of seismic traces into earth reflectivity series is known as deconvolution (Austin et al., 2018). Horizon separates rock layers with different depositional formations and reflection properties. The estimation of AI from the product of density and velocity provides details of reservoir characterization and the model-based inversion technique compensates for the loss of a low range of frequency components from the seismic data by creating an initial model applying a bandpass filter. The standard procedure in model-based inversion includes (i) wavelet estimation, (ii) seismic-to-well tie, (iii) horizon picking, (iv) initial model generation, (v) post-stack inversion analysis, and (vi) model-based inversion (Hampson et al., 2001). In figure 4a, the seismic section within 150-800 ms represents bed dips (10°-15°) from NW to SE direction, wells position (W1 and W2), picked horizons (H-I, H-II, H-III, H-IV), and a few identified faults (dashed lines).

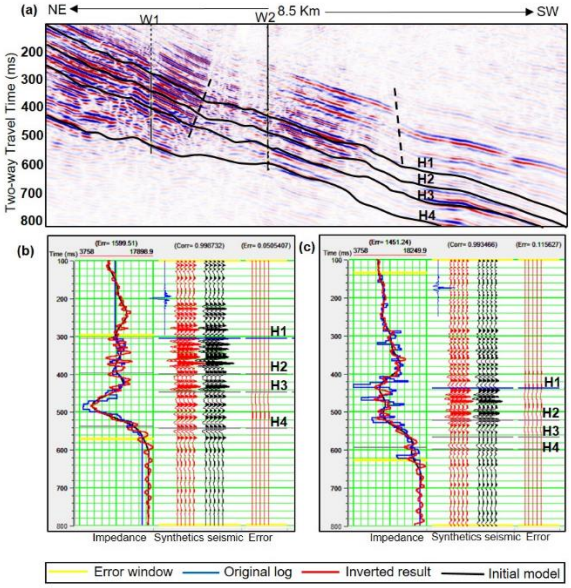

Figure 4. (a) 2D post-stack time migration seismic section within TWT 150-800 ms representing wells (W1 and W2), picked horizons (H1, H2, H3, H4), and faults (dashed lines), (b) post-stack inversion analysis of well W1 and, (c) post-stack inversion analysis of well W2, representing the original log, inverted results, initial, model, and analysis window.

The acquisition of seismic data in a particular frequency band has missing components of both low and high frequency. The low-frequency components contain useful information about the fluid and porosity in a reservoir which is necessary for obtaining better resolution during the inversion process. The impedance estimation of the initial model is absolute and sensitive to low-frequency components. Therefore, the use of a high-cut filter 10/15 Hz fills the missing frequency in the process of building an initial low-frequency AI model and interpolates along the horizon between the wells. In figure 5, the wavelet time and frequency response are compared between the seismic and the inverted data in the zone of interest from horizon H1 to H4. Figures 5a and 5b illustrate the amplitude spectrum in the time and frequency axis. The frequency of seismic data ranges from 20-120 Hz, while the inverted spectrum in figures 5c and 5d show the improvement in the frequency range containing dominant frequency below 10 Hz due to the application of a high-cut filter. The minimum misfit between the inverted synthetic and original log is necessary to optimize the inversion parameter of the seismic model at well locations. The best fit parameter gives a higher correlation between the inverted synthetic and original log data. The inversion analysis provides the final and best fit from the range of test parameters before initiating the inversion process in the seismic volume. In figures, 4b and 4c, the comparison between synthetic traces obtained from the inversion result with the input seismic trace, shows the correlation coefficient of 0.99 and 0.97 and measured error of 0.13 and 0.24 in well W1 and W2, respectively. Seismic attributes are the mathematical transformation of seismic trace

data. In this study, seismic attributes derived from post-stack inversion results, and petro-physical attributes obtained from well log data are used simultaneously. Subsequently, the seismic inversion attributes are integrated with petrophysical attributes to generate linear multivariate regression followed by non-linear NN methodology. The NN architecture provides better cross-correlation with reduced error compared to multivariate regression. Out of numerous seismic attributes generated, only a few contain meaningful information about reservoir properties and are useful in deriving petrophysical parameters by implementing NNs.

Neural network model

The attributes required to obtain NN models are distinguished into target attributes, training attributes, and final attributes. Attributes such as shale volume, Young's modulus, and Poisson's ratio as target attributes, and seismic inversion attributes are used as training attributes. A few examples of training attributes (inverted results) are quadrature trace, absolute amplitude, instantaneous frequency, instantaneous frequency, and many more. Hence, the specific training attributes having maximum cross-correlation, and minimum training and validation error becomes final attributes. The attributes with the minimum difference between training and validation error are considered for the estimation of shale volume, Young's modulus, and Poisson's ratio. Here, the same training data and attributes are tested in MLFN and PNN networks keeping W1 as training well and W2 as blind well for validation.

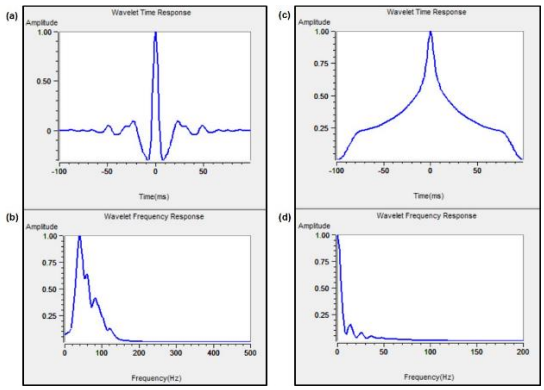

Figure 5. The wavelet time and frequency response are compared between the seismic and the inverted data in the zone of interest from horizon H1 to H4. (a) Amplitude spectrum versus time response of seismic data, (b) Amplitude spectrum versus frequency response of seismic data, (c) Amplitude spectrum versus time response of inverted seismic data and, (d) Amplitude spectrum versus frequency response of inverted seismic data.

The MLFN model consists of input, hidden, and output layer, where all layer constitutes a particular number of nodes that are connected with weights (Leiphart and Hart, 2001). The training in MLFN from well log data develops optimal weight between nodes, which yields the desired output. The weight is updated using the conjugate gradient optimization technique with a back-propagation procedure, the expression for the calculation of output layer:

$$Y = f\left[\alpha_0 + \sum_{j=1}^{n_2} \alpha_i f_i\left(\beta_{0j} + \sum_{i=1}^{n_1} \beta_{ij} x_i\right)\right], \quad (5)$$

Where Y and x are the output and input parameters, α and β act as connecting weights, n_1 and n_2 exhibit the dimension of the input vector and the number of hidden neurons. α_0 and β_{0j} are known as bias weights. The transfer function used in MLFN is a sigmoid function (f) and the common form of the function is:

$$sigmoid(a) = \frac{1}{1+e^{-a}}, \quad (6)$$

Where the value of "a" ranges between 0 and 1. The developed MLFN networks (1, 3, 5) consist of 70 input nodes linking 7 hidden nodes with 150 conjugate-gradient iterations that yield a single output layer. The cross-correlation measures the similarity between actual and predicted results.

The PNN architecture is a mathematical interpolation scheme that replaces the sigmoid transfer function in MLFN with an exponential function. PNN consists of input, pattern, summation, and output layer. The PNN is understood much better than MLFN by examining the mathematical expression in the analysis windows of the training data set consisting of a series of seismic samples and wells, where PNN represents the current output log in a linear combination of the log magnitude in the training data (Hampson et al., 2001). The current log magnitude *L(x)* is formulated as:

$$L(x) = \frac{\sum_{i=1}^{n} L_i e^{-(D(x,x_i))}}{\sum_{i=1}^{n} e^{-(D(x,x_i))}}, \quad (7)$$

Where, $D(x, x_i) = \sum_{j=1}^{m} \left(\frac{x_j - x_{ij}}{\sigma_j} \right)^2$, (8)

D(*x, xi*) denotes the distance between the input and each training point (*xi*) in multi-dimensional space, *n* is training examples from m attributes, *Li* is the measured target log values, *σj* is the smoothing parameter in the training of the network. The prediction error is controlled by the parameters *σj* which is minimized by applying a nonlinear conjugate gradient algorithm. Here, PNN networks (2, 4, 6) are tested with 25 smoothing parameters ranging from 0.1 to 3.0 comprising 100 iterations.

Results and Discussions

The cross-correlation, training, and validation error of MLFN and PNN networks compares the actual and predicted results for shale volume (Figure 6a and 6b), Young's modulus (Figure 6c and 6d), and Poisson's ratio (Figure 6e and 6f) is tabulated in table 2. Analysis from table 5 and figure 5 emphasizes that the MLFN model using networks-1 and 5 gives better results in shale volume and Poisson's ratio estimation (Figure 6a and 6e) whereas the PNN model uses network-4 yields effective Young's modulus output (Figure 6d). In the best shale volume, Young's modulus, and Poisson's ratio model, cross-correlation are 0.86, 0.96 and 0.85, training error are 0.09, 0.49 GPa and 0.01, validation error are 0.11, 0.92 GPa and 0.01, respectively.

Table 2. Comparison of six networks by implementing NN architectures in the estimation of the volume of shale, Young's modulus, and Poisson's ratio.

Estimated shale volume (V_{sh}) models				
Network	**Type**	**Cross-correlation**	**Training error**	**Validation error**
Network-1	MLFN	0.86	0.09	0.11
Network-2	PNN	0.8	0.1	0.12
Estimated Young's modulus (E) models				
Network	**Type**	**Cross-correlation**	**Training error**	**Validation error**
Network-3	MLFN	0.88	0.82 GPa	1.57 GPa
Network-4	PNN	0.96	0.49 GPa	0.92 GPa
Estimated Poisson's ratio (PR) models				
Network	**Type**	**Cross-correlation**	**Training error**	**Validation error**
Network-5	MLFN	0.85	0.01	0.01
Network-6	PNN	0.80	0.01	0.01

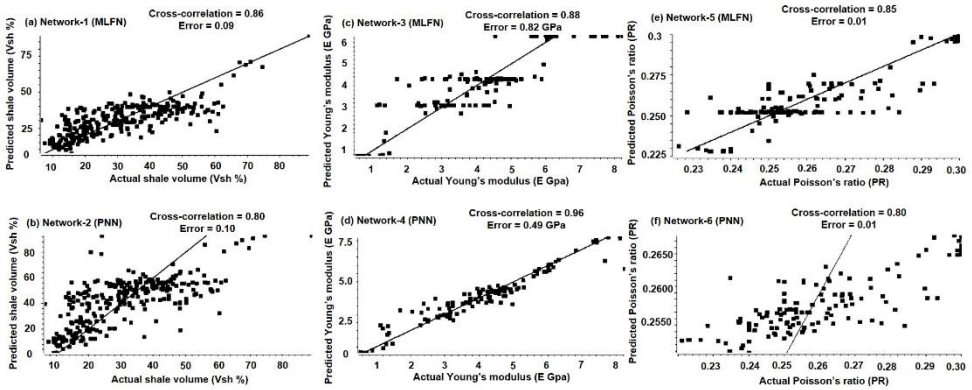

Figure 6. Cross-correlation between (i) actual and predicted shale volume (V_{sh}) mapping using (a) network-1 (MLFN) (b) network-2 (PNN); (ii) actual and predicted Young's modulus (E) mapping using (c) network-3 (MLFN) (d) network-4 (PNN) and; (iii) actual and predicted Poisson's ratio (PR) mapping using (e) network-5 (MLFN) (f) network-6 (PNN).

The AI section distinguishes coal, shale, and sandstone and identifies the top of the Barakar and Talchir formations. The relatively thicker coal seam (30-40 m) is better distinguished in the AI section compared to the thinner coal seam (1-10 m). In figure 7a, the color codes show AI ranges from 5000 to 16,000 (g/cc)*(m/s) in the reservoir. In shale, AI varies from 10000-16000 (g/cc)*(m/s), mix of sandstone and shale, it ranges from 5500-10000 (g/cc)*(m/s), and in coal, AI ranges from 5000-6000 (g/cc)*(m/s). The green color represents coal and the red/blue color represents lithology with higher shale content, while the yellow represents the mix of shale and sand. The best-mapped sections within 150-800 ms are represented in figures 7b, 7c, and 7d, respectively. The section in figure 7b shows the shale volume distribution from 15% to 55%. In coal, shale, and sandstone the distribution of shale volume is 15-20%, 30-35%, and 15-30% respectively. In figure 7c, Young's modulus ranges from 0.5 to 9.5 GPa, and it varies from 0.5-2.5 GPa, 6.5-9.5 GPa, and 4.0-6.0 GPa in coal, shale, and sandstone. In figure 7d, the Poisson's ratio ranges from 0.23 to 0.27, wherein coal, shale, and sandstone vary from 0.26-0.27, 0.23-0.25, and 0.24-0.26. The Young's modulus versus Poisson's ratio cross-plot in figure 8 classifies the coal, shale, and mix of sandstone and shale formations encircled based on brittle and ductile behaviour shown from (a) well log (W1 and W2) and (b) seismic section. Figure 8 illustrates the linear increase in brittleness with the increase in depth, as Young's modulus increases and Poisson's ratio decreases. The low Poison's ratio (0.23-0.24) and high Young's modulus (6.5-9.5 GPa) are brittle formations, that are relatively hard and rigid, which is seen in the shale formation whereas formations with a high Poisson's ratio (0.26-0.27) and low Young's modulus (0.5-2.5 GPa) are ductile with soft characteristics, which is observed in coal. The intermediate-range of Poisson's ratio (0.24-0.26) and Young's modulus (4.0-6.0 GPa) are formations containing a mix of sandstone and shale. The presence of higher shale volume in overlying and underlying coal seams acts as a good shale barrier due to its higher compressive strength and lower permeability for restricting the hydraulic fracturing fluid movement beyond the coal seam. High stiffness in the shale can withstand higher stress during hydraulic fracturing fluid injection. Thus, the demarcation of the shale layers provides information about continuity and extension. Young's modulus is associated with matrix shrinkage that affects the porosity, permeability, gas recovery rate, and in-situ stress condition of the coalbed methane reservoir. The seismic resolution depends on the wavelength, velocity, and frequency of seismic waves in the formation. However, the thinner coal seams are not effectively distinguishable in the section as the lower acoustic impedance of coal leads to higher reflectivity of acoustic waves from beds and lesser transmissivity to the sub-surface layer; and Rayleigh's limiting criteria for vertical resolution, where bed thickness is less than one-fourth the dominant wavelength cannot be resolved, hence bed thickness less than 10.0 m is not resolved. Moreover, the presence of cultural noise significantly affects the data quality.

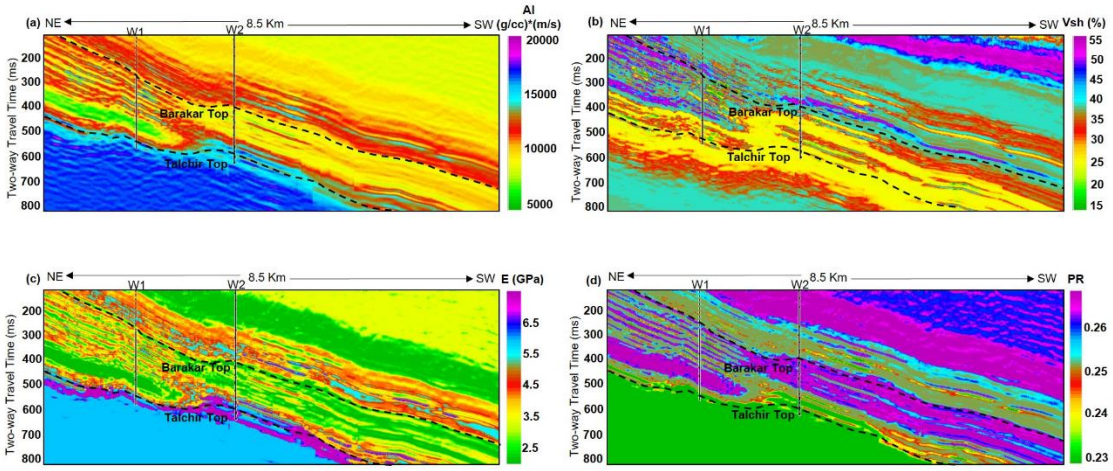

Figure 7. (a) Post-stack acoustic impedance (AI) inversion section representing AI magnitude ranging from 5000 to 16,000 (g/cc)*(m/s). (b) Shale volume (V_{sh}) distribution of MLFN model from 15-55 % in a reservoir. (c) Young's modulus (E) distribution of PNN model from 0.3-20 GPa in a reservoir. (d) Poisson's ratio (PR) distribution of MLFN model from 0.23-0.27 in a reservoir**.**

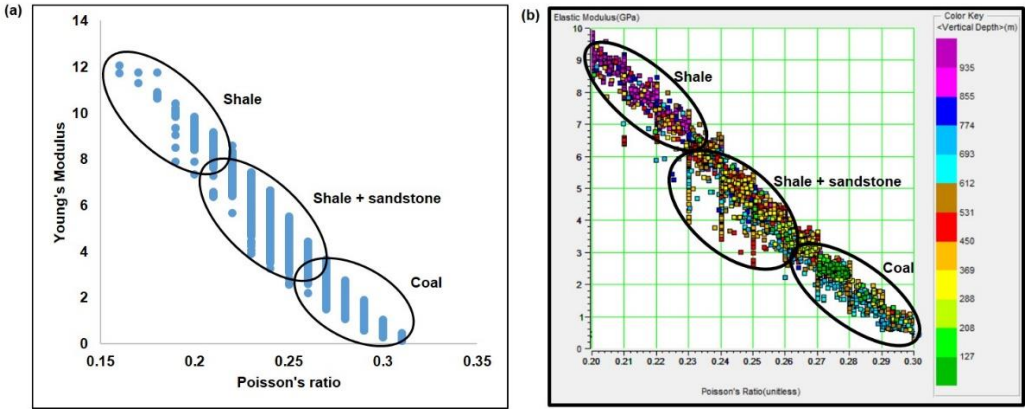

Figure 8. Poisson's ratio Vs. Young's modulus's cross-plot in the reservoir illustrates the encircled lithology of coal, shale, and a mix of shale and sandstone shown from (a) well log (W1 and W2) and (b) seismic section.

CONCLUSIONS

The following conclusion from the study are:

(1) Reservoir characterization using a model-based seismic inversion technique is attempted in the basin having data constraints. Based on acoustic impedance contrast the lithology is distinguishable in the reservoir, however, limitation exists in resolving thin coal seams that mainly depends on the frequency of seismic wave controlled by the geological factors. The use of seismic inversion attributes is vital in estimating reservoir properties and development planning for drilling successful wells and effective reservoir management.

(2) The application of non-linear relationships in the neural network provides effective results with minimum error. The best result selection depends on the cross-correlation between observed and predicted parameters of either MLFN or PNN models. The quantitative estimation of properties like modulus, and brittleness will provide crucial input for designing the hydro-fracturing job in the future for optimizing the gas production from this reservoir. Moreover, the derived reservoir properties from this study will help in further geomechanical analysis.

Acknowledgment

The author is thankful to Oil and Natural Gas Corporation Limited, India for supporting us to conduct the research work. The author is also grateful to Mr. Aditya Johri, ED-Asset Manager (CBM) for the support and encouragement for the research work. The author is also thankful to Mr. Gautam Bhattacharya (Chief Geologist), ONGC, and all executives of Logging Services, CBM Asset Bokaro.

References

Austin, O., Onyekuru, S.O., Ebuka, O.A., and Abdulrazzaq, T.Z. (2018) Application of model-based inversion technique in a field in the coastal swamp depo belt, Niger delta. International journal of advanced geosciences, v.6(1), pp.122-126.

Banerjee, A., and Chatterjee, R. (2021) A Methodology to Estimate Proximate and Gas Content Saturation with Lithological Classification in Coalbed Methane Reservoir, Bokaro Field, India. Natural Resources Research, v.30, pp.2413-2429. https://doi.org/10.1007/s11053-021-09828-2.

Bateman, R.M. (1985) Openhole Log Analysis and Formation Evaluation. Pretice Hall PTR, New Jersey, pp. 647.

Boonen, P. (2003) Advantages and challenges of using logging-while-drilling data in rock mechanical log analysis and wellbore stability modeling. *In*: Proceedings AADE National Technology Conference, Texas; 1–3 April 2003.

Ghosh, S.C. (2002) The Raniganj Coal Basin: an example of an Indian Gondwana rift. Sedimentary Geology, v.147, pp.155-176. https://doi.org/10.1016/S0037-0738(01)00195-6

Hampson, D., Schuelke, J., and Quirein, J. (2001) Use of multi-attribute transforms to predict log properties from seismic data. Geophysics, v.66, pp.220-236.

Leiphart, D., and Hart, B.S. (2001). Comparison of linear regression and a probabilistic neural network to predict porosity from 3-d seismic attributes in lower brushy canyon channeled sandstones, Southeast New Mexico. Geophysics, v.66, pp.1349-1358.

Mallick, S. (1995) Model-based inversion of amplitude-variations-with-offset data using a genetic algorithm. Geophysics, v.60(4), pp.939-954.

Saggaf, M.M., Toksoz, M.N., and Mustafa, H.M. (2003) Estimation of Reservoir Properties from Seismic Data by Smooth Neural Networks. Geophysics, v.68, pp.1969-1983. https://org.doi./10.1190/1.1635051